# Research Report May 2025
# The Subducting of Oceanic Sediments through the Lower Mantle to the Core-Mantle Boundary

Elena-Marie Rogmann, Takayuki Ishii [1]

[1]: Institute for Planetary Materials, Okayama University, Okayama, Japan

## Research Purpose

Sedimentary phase relations are an important component of subducting slabs. However, when compared to the other constituents of subducting slabs, high pressure phase relation data remains significantly sparser (Irifune et al., 1994; Ono, 1998; Rapp et al., 2008; Wu et al., 2009; Ishii et al., 2012; Zhang et al., 2016). Traditionally, upper continental crust (UCC) compositions (e.g. Irifune et al.; Wu et al.; Ishii et al.; Zhang et al.) have been used to probe sedimentary phase relations throughout the mantle. The phase relations of the marine sedimentary material (GLOSS – Global Subducted Sediment), have not previously been used for mantle phase relation studies (Brey et al., 2015), exceeding arc melting conditions. Further, there are no phase relation studies on any sedimentary compositions exceeding 28 GPa (Ishii et al., 2012). A composition like GLOSS is applicable for those subducting slabs in which the sedimentary component remains essentially unaltered. However, in some subducting slabs, sediments undergo partial melting (e.g. Zhang et al., 2016; Förster and Selway, 2021; Turner and Langmuir, 2022) and, therefore, a melt depleted sedimentary composition ('restite') composition remains in the slab (Mazzone et al., 1989) and may be transported into the deep Earth instead. For restite compositions, phase relations at conditions even just exceeding those of partial melting, during the onset of subduction, remain unprobed. Overall, understanding the behaviour of sediments or their products throughout a range of mantle conditions is important for building a mineral physical model of the Earth's mantle, as well as for understanding the heat dynamics of the deep Earth, as sediments contain a large amount of radiogenic $^{40}$K (Plank and Langmuir, 1998; Plank, 2014). Additionally, understanding the behaviour of sediments in the deep is crucial for understanding geochemical cycling throughout the Earth, as well as its chemical evolution.

# Actually conducted Research

Since commencing experiments at the IPM in early 2025, GLOSS II starting materials were prepared and used in multi anvil experiments (Table 1). This includes dry and wet GLOSS II (Plank, 2014) powder. The wet GLOSS II contains 2 wt.% $H_2O$, added as $Al(OH)_3$. The dry GLOSS II starting material was subjected to NNO conditions during three rounds of gas mixing for a minimum of 6 hours with 298 cc/min $CO_2$ and 2 cc/min $H_2$. For 10/4 multi anvil experiments, dry Ni:NiO oxide powder was added to the dry GLOSS II starting material, and Ni:$Ni(OH)_2$ to the wet GLOSS II starting material. The oxygen fugacity buffer materials were spatially separated from the sample material (Figure 2). The buffer materials were not added for 8/3 experiments (Figure 2). A second set of starting materials has been used for multi anvil experiments. Those starting materials have compositions of clay and clay restite (generated at 3 GPa and 800 °C, leading to 50 % melt extraction, Table 1) and were prepared as glasses (Skora and Blundy, 2010). Dry samples were prepared in AuPd foil capsules, wet samples in welded Pt capsules (Figure 2). An overview of the starting material compositions can be found in Table 1. All multi anvil experiments were conducted in the 1000-ton press at the Institute for Planetary Materials (IPM) of Okayama University in Misasa, Japan, using assembly designs outlined in Figure 1. An overview of the experiments and their run conditions is provided in Table (Table 2). The run products of successful multi anvil experiments have been polished and probed by means of X-ray diffraction (XRD) and scanning electron microscopy (SEM).

Table 1: Compositions of starting materials used in multi anvil experiments for the present study with UCC (Upper continental crust composition), used in previous experiments, for reference. GLOSS II (Plank, 2014) was used both dry and with 2 wt.% $H_2O$. The Clay and Clay restite are those of (Skora and Blundy, 2010).

| | UCC | GLOSS II | Clay | Clay Restite |
|---|---|---|---|---|
| $SiO_2$ | 66 | 63.22 | 61.62 | 46.90 |
| $TiO_2$ | 0.5 | 0.71 | 1.00 | 1.60 |
| $Al_2O_3$ | 15.2 | 13.97 | 19.04 | 24.30 |
| FeO | 4.5 | 6.33 | 8.92 | 16.50 |
| MnO | 0.08 | 0.48 | | |
| MgO | 2.2 | 3.07 | 3.91 | 7.40 |
| CaO | 4.2 | 6.95 | 1.80 | 2.70 |
| $Na_2O$ | 3.9 | 2.79 | 2.00 | 0.60 |
| $K_2O$ | 3.4 | 2.47 | 1.70 | 0.00 |

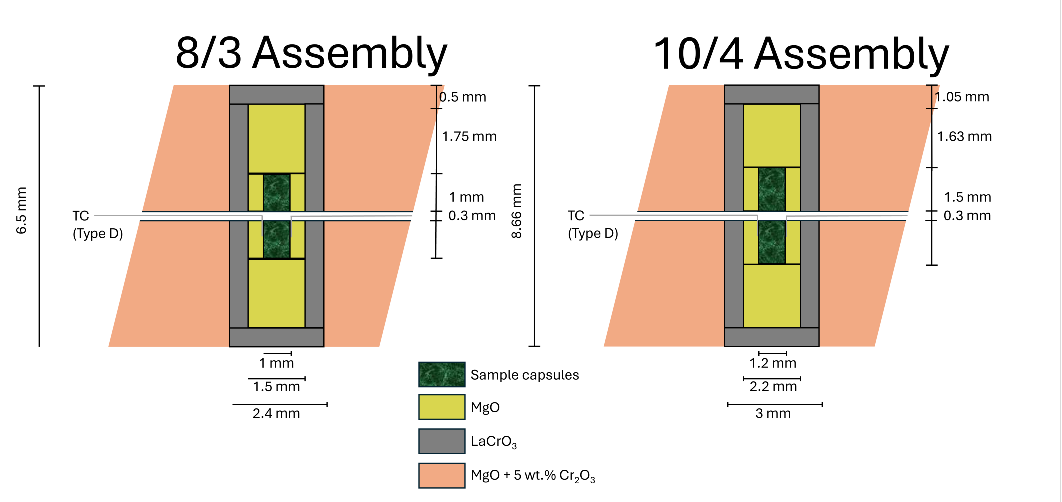

Figure 1: Multi anvil assemblies used for the experiments.

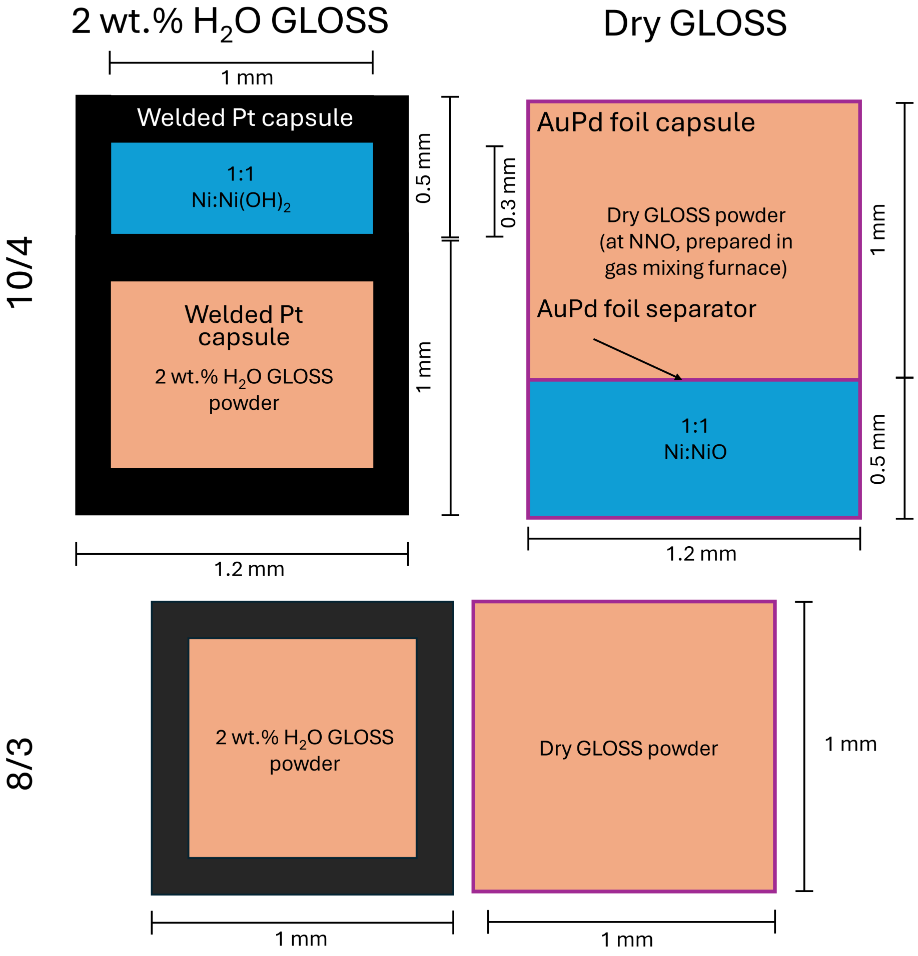

Figure 2: Capsules used for the multi anvil experiments. Top row: 10/4 experiments; Bottom row: 8/3 experiments. The water bearing starting materials are contained in welded Pt-capsules, the dry starting material in AuPd foil. NNO oxygen fugacity buffer material is placed next to the starting material in 10/4 experiments, spatially separated either in a separately welded compartment in the case of Pt, or by a sheet of AuPd.

Table 2: Overview of the multi anvil experiments conducted at IPM in the report period. Exp.: Experiment; P: Pressure; T: Temperature. Size denotes the assembly size. All experiments were conducted with F08 cubes and $LaCrO_3$ heaters. SM: Starting Material; Cap.: Capsule material.

| Exp. No. | P [GPa] | Load [MN] | T[°C] | Time [h] | Size | SM1 | Cap. 1 | SM2 | Cap. 2 | Notes |
|---|---|---|---|---|---|---|---|---|---|---|
| Ik3995 | 18 | 5.5 | 1500 | 4.5 | 10_4 | dry GLOSS | Pt | wet GLOSS | Pt | |
| Ik4005 | 18 | 5.5 | - | - | 10_4 | dry GLOSS | Pt | wet GLOSS | Pt | Heater failed |
| Ik4011 | 18 | 5.5 | 1200 | 4 | 10_4 | dry GLOSS | Pt | wet GLOSS | Pt | |
| Ik4015 | 20 | 6.1 | 1500 | 3.3 | 10_4 | dry GLOSS | Pt | wet GLOSS | Pt | |
| Ik4020 | 20 | 6.1 | 1300 | 4 | 10_4 | Clay | AuPd | Restite | AuPd | |
| Ik4025 | 20 | 6.1 | 1600 | 4 | 10_4 | Clay | AuPd | Restite | AuPd | |
| Ik4028 | 20 | 6.1 | 1200 | 4 | 10_4 | dry GLOSS (NNO) | AuPd | wet GLOSS | Pt | |
| Ik4037 | 24 | 7 | 1300 | 4 | 8_3 | dry GLOSS (NNO) | AuPd | wet GLOSS | Pt + AuPd | |
| Ik4044 | 25 | 8 | 1600 | 5 | 8_3 | Clay | AuPd | Restite | AuPd | |
| IK4046 | 20 | 6.1 | - | - | 10_4 | dry GLOSS (NNO) | AuPd | wet GLOSS | Pt | Heater failed |
| Ik4056 | 20 | 6.1 | - | - | 10_4 | dry GLOSS (NNO) | AuPd | wet GLOSS | Pt | Heater failed |
| Ik4063 | 24 | 7 | - | - | 8_3 | dry GLOSS (NNO) | AuPd | wet GLOSS | Pt + AuPd | Blowout |
| Ik4067 | 24 | 7 | - | - | 8_3 | dry GLOSS (NNO) | AuPd | wet GLOSS | Pt | Heater failed |

# Research Outcomes

The experiments conducted so far at the IPM contribute to two research projects under the sedimentary phase relations umbrella. 1) Is a classic multi anvil phase relation study of dry and hydrous GLOSS II at a range of pressure and temperature conditions and 2) are multi anvil experiments to supplement pre-existing diamond anvil cell data of high pressure phase relations of clay and clay-restite.

## 1) The phase relations of dry and wet GLOSS-II at high pressures and temperatures

In this ongoing project, we determine the phase relations of dry and water bearing (2 wt.% $H_2O$) GLOSS compositions at a range of mantle relevant pressures and temperatures. The determined stable phase relations are reported in Figure 3, and the corresponding phase compositions are provided in Table 3. Temperatures between a mantle geotherm (Ganguly et al., 2009) and an estimated sedimentary geotherm (Estimate based on Ganguly et al. (2009)) are applied. Due to sluggish phase transitions the very coldest sedimentary slab temperatures are avoided in this experimental campaign.

Table 3: Overview of the mineral phase compositions obtained by SEM from the multi anvil experiments on the dry and wet GLOSS-II compositions, reported in cations per formula unit. The dry experiment at 20 GPa and 1500 °C requires further polishing preceeding definitive chemical analysis. Cpx: Clinopyroxene; K-Holl: K-Hollandite; Stish: Stishovite; CaPv: Ca-perovskite; CAS: Calcium-aluminium rich phase; Egg: Phase Egg; $\delta$: delta phase; NAL: New aluminous phase; P: Pressure; T: Temperature.

| | **P [GPa]** | **T [C]** | | **Si** | **Ti** | **Al** | **Mg** | **Mn** | **Fe** | **Ca** | **Na** | **K** | **O** |
|---|---|---|---|---|---|---|---|---|---|---|---|---|---|
| Dry | 18 | 1500 | Garnet | 3.42 | 0.04 | 1.59 | 0.72 | 0 | 1 | 1.00 | 0.48 | 0 | 12 |
| Dry | 18 | 1200 | Garnet | 3.22 | 0 | 1.83 | 0.65 | 0 | 0.79 | 1.19 | 0.36 | 0 | 12 |
| Dry | 20 | 1200 | Garnet | 3.53 | 0 | 2.03 | 0.69 | 0 | 0.91 | 0.00 | 0.59 | 0 | 12 |
| Dry | 24 | 1300 | Garnet | 3.34 | 0 | 1.70 | 1.45 | 0.10 | 0.65 | 0.39 | 0.36 | 0 | 12 |
| Wet | 18 | 1500 | Garnet | 3.14 | 0.09 | 1.70 | 0.73 | 0.11 | 0.76 | 1.21 | 0.33 | 0 | 12 |
| Wet | 18 | 1200 | Garnet | 3.41 | 0 | 1.62 | 0.75 | 0 | 0.63 | 1.18 | 0.39 | 0 | 12 |
| Wet | 20 | 1200 | Garnet | 3.32 | 0 | 1.69 | 0.81 | 0 | 0.71 | 1.17 | 0.25 | 0 | 12 |
| Wet | 20 | 1500 | Garnet | 3.27 | 0 | 1.72 | 0.81 | 0 | 0.78 | 1.12 | 0.34 | 0 | 12 |
| Dry | 18 | 1200 | Cpx | 2.19 | 0 | 0.81 | 0 | 0 | 0 | 0 | 0.84 | 0 | 6 |
| Wet | 18 | 1500 | Cpx | 1.48 | 0 | 0.67 | 0.18 | 0 | 0.88 | 0.98 | 0 | 0 | 6 |
| Dry | 18 | 1500 | K-Holl | 2.99 | 0 | 1.02 | 0 | 0 | 0 | 0.02 | 0.19 | 0.74 | 8 |
| Dry | 18 | 1200 | K-Holl | 3.03 | 0 | 0.98 | 0 | 0 | 0 | 0 | 0.12 | 0.85 | 8 |
| Dry | 20 | 1200 | K-Holl | 2.92 | 0 | 1.06 | 0 | 0 | 0 | 0.26 | 0 | 0.61 | 8 |
| Dry | 24 | 1300 | K-Holl | 2.95 | 0 | 1.11 | 0 | 0 | 0 | 0.00 | 0 | 0.71 | 8 |
| Wet | 18 | 1500 | K-Holl | 2.93 | 0 | 1.06 | 0 | 0 | 0 | 0.10 | 0.16 | 0.73 | 8 |
| Wet | 18 | 1200 | K-Holl | 3.03 | 0 | 0.99 | 0 | 0 | 0 | 0 | 0.11 | 0.80 | 8 |
| Wet | 20 | 1200 | K-Holl | 3.01 | 0 | 1.03 | 0 | 0 | 0 | 0 | 0 | 0.85 | 8 |
| Wet | 20 | 1500 | K-Holl | 2.94 | 0 | 1.08 | 0 | 0 | 0 | 0.05 | 0.16 | 0.72 | 8 |
| Wet | 24 | 1300 | K-Holl | 2.98 | 0 | 1.08 | 0 | 0 | 0 | 0 | 0 | 0.82 | 8 |
| Dry | 18 | 1500 | Stish | 0.98 | 0 | 0.02 | 0 | 0 | 0 | 0 | 0 | 0 | 2 |
| Dry | 18 | 1200 | Stish | 1.00 | 0 | 0.01 | 0 | 0 | 0 | 0 | 0 | 0 | 2 |
| Dry | 20 | 1200 | Stish | 1.00 | 0 | 0 | 0 | 0 | 0 | 0 | 0 | 0 | 2 |
| Dry | 24 | 1300 | Stish | 0.96 | 0 | 0.05 | 0 | 0 | 0 | 0 | 0 | 0 | 2 |
| Wet | 18 | 1500 | Stish | 0.98 | 0 | 0.02 | 0 | 0 | 0 | 0 | 0 | 0 | 2 |
| Wet | 18 | 1200 | Stish | 0.99 | 0 | 0.01 | 0 | 0 | 0 | 0 | 0 | 0 | 2 |
| Wet | 20 | 1200 | Stish | 1.00 | 0 | 0.00 | 0 | 0 | 0 | 0 | 0 | 0 | 2 |
| Wet | 20 | 1500 | Stish | 0.98 | 0 | 0.03 | 0 | 0 | 0 | 0 | 0 | 0 | 2 |
| Wet | 24 | 1300 | Stish | 0.96 | 0 | 0.06 | 0 | 0 | 0 | 0 | 0 | 0 | 2 |
| Dry | 20 | 1200 | CF | 0.81 | 0 | 1.17 | 0.12 | 0 | 0.16 | 0 | 0.68 | 0 | 4 |
| Dry | 24 | 1300 | CF | 0.49 | 0 | 1.46 | 0.52 | 0 | 0.10 | 0 | 0.30 | 0.05 | 4 |
| Dry | 18 | 1200 | CaPv | 0.53 | 0.48 | 0.05 | 0 | 0 | 0 | 0.92 | 0 | 0 | 3 |
| Wet | 18 | 1200 | CaPv | 0.63 | 0.43 | 0 | 0 | 0 | 0 | 0.88 | 0 | 0 | 3 |
| Wet | 20 | 1200 | CaPv | 0.64 | 0.36 | 0 | 0 | 0 | 0 | 1.00 | 0 | 0 | 3 |
| Wet | 24 | 1300 | CaPv | 0.95 | 0.04 | 0.05 | 0 | 0 | 0 | 0.95 | 0 | 0 | 3 |
| Dry | 18 | 1500 | CAS | 2.33 | 0 | 3.56 | 0.01 | 0 | 0.05 | 0.75 | 0 | 0.08 | 11 |
| Dry | 24 | 1300 | CAS | 2.40 | 0 | 3.46 | 0.13 | 0 | 0.00 | 0.75 | 0.16 | 0.12 | 11 |
| Wet | 20 | 1500 | CAS | 2.34 | 0 | 3.59 | 0.00 | 0 | 0 | 0.78 | 0.18 | 0.11 | 11 |
| Wet | 24 | 1300 | CAS | 2.41 | 0 | 3.44 | 0.16 | 0 | 0 | 0.79 | 0 | 0.15 | 11 |
| Wet | 18 | 1500 | Egg | 1.12 | 0.03 | 1.10 | 0 | 0 | 0.05 | 0 | 0 | 0 | 4 |
| Wet | 18 | 1200 | Egg | 1.15 | 0 | 1.13 | 0 | 0 | 0 | 0 | 0 | 0 | 4 |
| Wet | 18 | 1200 | $\delta$ | 0.12 | 0 | 1.11 | 0.07 | 0 | 0.02 | 0 | 0 | 0 | 2 |
| Wet | 20 | 1200 | $\delta$ | 0.58 | 0 | 0.56 | 0 | 0 | 0 | 0 | 0 | 0 | 2 |
| Dry | 24 | 1300 | NAL | 0.68 | 0 | 1.28 | 0.27 | 0 | 0.12 | 0.03 | 0.60 | 0 | 4 |
| Wet | 24 | 1300 | NAL | 0.52 | 0 | 1.40 | 0.62 | 0 | 0.03 | 0.08 | 0.11 | 0.11 | 4 |

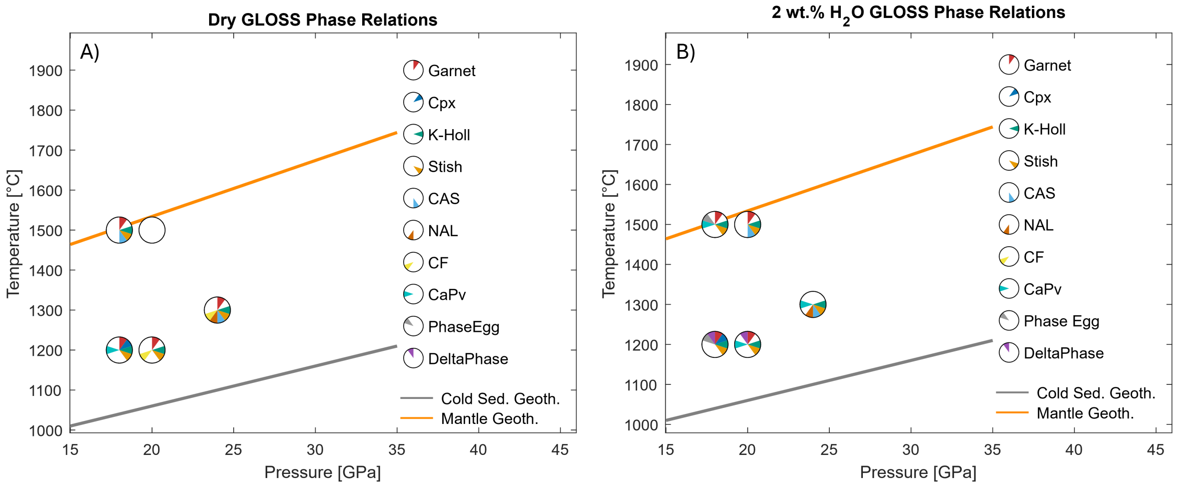

Figure 3: Preliminary A) Dry and B) Wet (2 wt. $H_2O$) GLOSS phase relation data. Eventhough no hydrous phases are expected for the dry composition, the same positions were used for both figures for simplicity. Both geotherms are used based on Ganguly et al. (2009), with the cold sediment geotherm being an interpolation of their data. As sediments form the very top of subducting slabs, they may be at a temperature very close to the surrounding mantle. The dry experiment at 20 GPa and 1500 °C remains to be properly analysed, as further polishing is required.

The dry phase relations and compositions from experiment 1k4015, conducted at 20 GPa and 1500 °C) are still missing from the phase composition overview (Table 3, Figure 3), as the polishing needs further work. Further, hydrous phases have yet to be identified in the wet samples of runs 14015 and 1k4037, conducted at 20 GPa with 1500 °C and 24 GPa with 1300 °C, respectively. For this, the sample capsule will be polished further, in order to sample different areas of the capsule, in case certain phases concentrated in different regions of the capsule, possibly due to minor temperature gradients.

Notably, Calcium-ferrite type (CF) phase has not been observed in any water-bearing experiments so far, in accordance with the observations of Ishii et al. (2023) and Zhang et al. (2025).

**Future Work** on this project will include expanding the pressure and temperature range of these experiments. Additionally, chemical compositional data is going to be collected by EPMA and will be reported, including propagated uncertainties. The chemical compositions as a function of pressure and temperature will be visualised once compositional data is finalised and more pressure points have been collected. Phase relation experiments are also to be conducted on dry and wet GLOSS restite composition, after the corresponding restite composition has been determined at 3 GPa. While the initial restite composition on first formation is expected to be dry, as all volatiles will be lost during arc melting, such restite compositions may be rehydrated during deeper subduction from deeper slab layers. Additionally, phase proportions will be determined by mass balance and visually, using ImageJ.

## 2) The Phase Relations of Clay and Clay Restite to 80 GPa

The second array of experiments is being conducted to supplement previously collected synchrotron XRD diamond anvil cell (DAC) data with chemical compositional data. The DAC experiments were conducted at pressures ranging from 9-80 GPa on the clay and the restite composition (Table 1). In order to supplement this XRD study with the compositions of the minerals, first, reproducibility between the DAC and MA experiments had to be established. In order to ascertain this, experiments were run at pressure conditions that had also been used in the diamond anvil cell experiments. In order to facilitate crystal growth sufficient for measurement by SEM and EPMA, slightly higher temperatures than used in the diamond anvil cell study had to be applied. At comparable pressure conditions, the same phases were observed in the XRD of both the DAC and the multi anvil experiments (Figure 4).

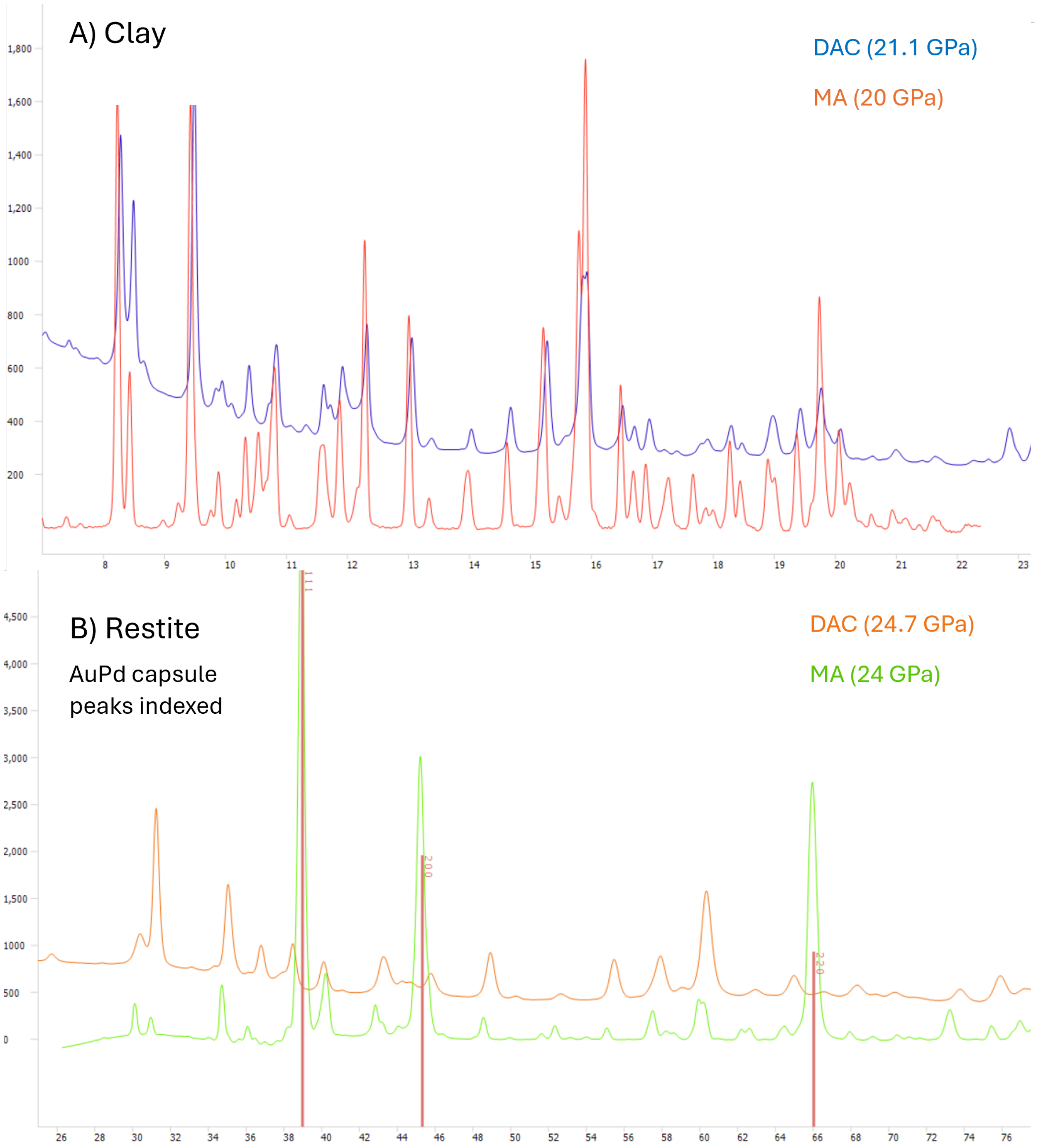

Figure 4: Comparison between the XRD patterns collected for A) Clay and B) Restite between the experiments conducted by DAC and multi anvil press. Due to a strong signal from the AuPd capsule material in the multi anvil restite experiment, the AuPd peaks are indexed. The patterns for both respective experiments are in good agreement with each other.

The preliminary phase relations are provided in Figure 5. They show a lot of dynamic phase changes for both compositions in the mantle transition zone into the topmost lower mantle. At higher pressures, the only observed changes are the loss of the NAL phase for the restite composition between 34 and 43 GPa, as well as the loss of K-Hollandite between 42 and 53 GPa (Figure 5) for the clay composition. These changes in phase relations have to be explained by shifts in solubility of alkali elements and alumina, of the remaining stable phases.

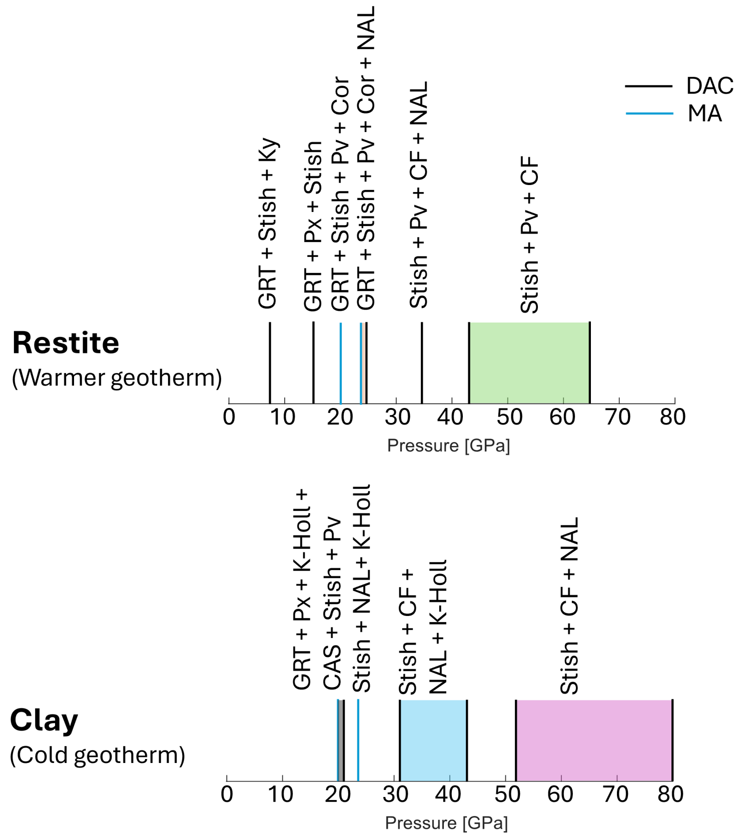

Figure 5: Preliminary high pressure phase relations obtained for clay and clay restite compositions. Lines in blue indicate phase relations as obtained from multi anvil experiments, lines in black indicate DAC experiments. Shaded regions indicate no change in phase assemblage between their pressure anchors.

The preliminary SEM obtained compositions of the observed phases are provided in Table 4. Most notably, as Mg-perovskitein restite becomes more abundant between 20-24 GPa, the composition shifts to significantly less Ti- and Fe-rich compositions, similar to the Ti-rich first occurrences of Ca-perovskite (e.g. Ono et al., 2001; Hirose and Fei, 2002; Ishii et al., 2019).

Table 4: Compositions of the mineral phases present in the experiments on the clay and clay restite compositions. All compositions are reported in cations per formula unit. Stish: Stishovite; Cor: Corundum; Pv: Perovskite; K-Holl: K-Hollandite; NAL: New Aluminous Phase.

| Exp. | SM | P [GPa] | Phase | Si | Ti | Al | Mg | Fe | Ca | Na | K | O | Si+Ti+Al | Mg+Fe+Ca+Na+K |
|---|---|---|---|---|---|---|---|---|---|---|---|---|---|---|
| Ik4025 | Restite | 20 GPa | Stish | 0.92 | 0 | 0.09 | 0.01 | 0.01 | 0 | 0 | 0 | 2 | 1.01 | 0.02 |
| Ik4044 | Restite | 24 GPa | Stish | 0.95 | 0 | 0.06 | 0 | 0 | 0 | 0 | 0 | 2 | 1.02 | 0 |
| Ik4025 | Clay | 20 GPa | Stish | 0.96 | 0 | 0.05 | 0 | 0.01 | 0 | 0 | 0 | 2 | 1.01 | 0.01 |
| Ik4044 | Clay | 24 GPa | Stish | 0.97 | 0 | 0.04 | 0 | 0 | 0 | 0 | 0 | 2 | 1.01 | 0 |
| Ik4025 | Restite | 20 GPa | Cor | too fine grained | | | | | | | | | | 0 |
| Ik4044 | Restite | 24 GPa | Cor | too fine grained | | | | | | | | | | 0 |
| Ik4025 | Restite | 20 GPa | Garnet | 3.16 | 0.04 | 1.80 | 1.13 | 1.36 | 0.35 | 0.13 | 0 | 12 | 5.00 | 2.96 |
| Ik4044 | Restite | 24 GPa | Garnet | 3.11 | 0 | 1.88 | 1.42 | 1.14 | 0.35 | 0.10 | 0 | 12 | 4.99 | 3.01 |
| Ik4025 | Clay | 20 GPa | Garnet | 3.53 | 0.09 | 1.51 | 0.90 | 1.17 | 0.24 | 0.37 | 0 | 12 | 5.13 | 2.68 |
| Ik4025 | Clay | 20 GPa | FeTi Pv | 0.29 | 0.47 | 0.40 | 0.13 | 0.75 | 0.01 | 0 | 0 | 3 | 1.15 | 0.89 |
| Ik4044 | Restite | 24 GPa | FeTi Pv | 0.55 | 0.13 | 0.47 | 0.39 | 0.55 | 0 | 0 | 0 | 3 | 1.15 | 0.94 |
| Ik4025 | Clay | 20 GPa | K-Holl | 2.96 | 0.02 | 1.03 | 0 | 0.03 | 0.05 | 0.22 | 0.64 | 8 | 4.01 | 0.94 |
| Ik4044 | Clay | 24 GPa | K-Holl | 2.98 | 0 | 1.06 | 0 | 0 | 0 | 0.07 | 0.81 | 8 | 4.04 | 0.89 |
| Ik4044 | Clay | 24 GPa | NAL | 0.63 | 0.03 | 1.19 | 0.34 | 0.37 | 0.03 | 0.19 | 0.08 | 4 | 1.86 | 1.01 |

**Further experiments** will be conducted at 32 GPa and 40 GPa. Those will primarily aim to target the pressure dependence of bridgmanite composition and the effect of the absence of NAL on the compositions of the remaining phases in the restite. For the clay, we aim to identify whether CF becomes K-host phase, as K-Hollandite disappears from the clay phase assemblage (Figure 5), as observed for pure aluminous phase systems (Rogmann et al., 2024). Additionally, EPMA measurements will be necessary to finalise the compositional results and phase proportions will be determined by Rietveld refiment for the DAC data and mass balance calculations for the multi anvil data.

# References

Brey, G., Girnis, A., Bulatov, V., Höfer, H., Gerdes, A., and Woodland, A. (2015). Reduced sediment melting at 7.5–12 GPa: phase relations, geochemical signals and diamond nucleation. *Contributions to Mineralogy and Petrology*, 170:1–25.

Förster, M. and Selway, K. (2021). Melting of subducted sediments reconciles geophysical images of subduction zones. *Nature Communications*, 12(1):1320.

Ganguly, J., Freed, A. M., and Saxena, S. K. (2009). Density profiles of oceanic slabs and surrounding mantle: Integrated thermodynamic and thermal modeling, and implications for the fate of slabs at the 660 km discontinuity. *Physics of the Earth and Planetary Interiors*, 172(3-4):257–267.

Hirose, K. and Fei, Y. (2002). Subsolidus and melting phase relations of basaltic composition in the uppermost lower mantle. *Geochimica et Cosmochimica Acta*, 66(12):2099–2108.

Irifune, T., Ringwood, A. E., and Hibberson, W. O. (1994). Subduction of continental crust and terrigenous and pelagic sediments: an experimental study. *Earth and Planetary Science Letters*, 126(4):351–368.

Ishii, T., Criniti, G., Wang, X., Glazyrin, K., and Boffa Ballaran, T. (2023). Synthesis and structural analysis of $CaFe_2O_4$-type single crystals in the $NaAlSiO_4$-$MgAl_2O_4$-$Fe_3O_4$ system. *American Mineralogist*, 108(1):217–221.

Ishii, T., Kojitani, H., and Akaogi, M. (2012). High-pressure phase transitions and subduction behavior of continental crust at pressure–temperature conditions up to the upper part of the lower mantle. *Earth and Planetary Science Letters*, 357:31–41.

Ishii, T., Kojitani, H., and Akaogi, M. (2019). Phase relations of Harzburgite and MORB up to the uppermost lower mantle conditions: Precise comparison with Pyrolite by multisample cell high-pressure experiments with implication to dynamics of subducted slabs. *Journal of Geophysical Research: Solid Earth*, 124(4):3491–3507.

Mazzone, P. et al. (1989). Peraluminous xenoliths in kimberlite: metamorphosed restites produced by partial melting of pelites. *Geochimica et Cosmochimica Acta*, 53(7):1551–1561.

Ono, S. (1998). Stability limits of hydrous minerals in sediment and mid-ocean ridge basalt compositions: Implications for water transport in subduction zones. *Journal of Geophysical Research: Solid Earth*, 103(B8):18253–18267.

Ono, S., Ito, E., and Katsura, T. (2001). Mineralogy of subducted basaltic crust (MORB) from 25 to 37 GPa, and chemical heterogeneity of the lower mantle. *Earth and Planetary Science Letters*, 190(1-2):57–63.

Plank, T. (2014). The chemical composition of subducting sediments. Elsevier.

Plank, T. and Langmuir, C. H. (1998). The chemical composition of subducting sediment and its consequences for the crust and mantle. *Chemical geology*, 145(3-4):325–394.

Rapp, R. P., Irifune, T., Shimizu, N., Nishiyama, N., Norman, M. D., and Inoue, T. (2008). Subduction recycling of continental sediments and the origin of geochemically enriched reservoirs in the deep mantle. *Earth and Planetary Science Letters*, 271(1-4):14–23.

Rogmann, E.-M., Jennings, E. S., Ross, J., Miyajima, N., Walter, M. J., Kohn, S. C., and Lord, O. T. (2024). The effect of potassium on aluminous phase stability in the lower mantle. *Contributions to Mineralogy and Petrology*, 179(5):1–18.

Skora, S. and Blundy, J. (2010). High-pressure hydrous phase relations of radiolarian clay and implications for the involvement of subducted sediment in arc magmatism. *Journal of Petrology*, 51(11):2211–2243.

Turner, S. J. and Langmuir, C. H. (2022). Sediment and ocean crust both melt at subduction zones. *Earth and Planetary Science Letters*, 584:117424.

Wu, Y., Fei, Y., Jin, Z., and Liu, X. (2009). The fate of subducted upper continental crust: an experimental study. *Earth and Planetary Science Letters*, 282(1-4):275–284.

Zhang, X., Mashino, I., and Ishii, T. (2025). Stability and water solubility of calcium ferrite-type aluminum-rich phase: implications for deep water cycle caused by subducting basaltic crusts. *Progress in Earth and Planetary Science*, 12(1):1–12.

Zhang, Y., Wu, Y., Wang, C., Zhu, L., and Jin, Z. (2016). Experimental constraints on the fate of subducted upper continental crust beyond the “depth of no return”. *Geochimica et Cosmochimica Acta*, 186:207–225.